

## Preparation and photocatalytic activity of apatite-precipitated TiO<sub>2</sub>

K. Soysal<sup>a</sup>, J. Park<sup>b</sup>, S.H. You<sup>c,\*</sup>, D.W. Shin<sup>c</sup>, W.T. Bae<sup>c</sup> and A. Ozturk<sup>a</sup>

<sup>a</sup>Department of Metallurgical and Materials Engineering, Middle East Technical University, Ankara, 06531 Turkey

<sup>b</sup>Department of Materials Engineering, Atilim University, Ankara, 06836 Turkey

<sup>c</sup>Division of Advanced Materials Science and Engineering, Engineering Research Institute, Gyeongsang National University, Jinju, Gyeongnam, 660-701 Korea

Apatite was precipitated on the surface of titanium dioxide (TiO<sub>2</sub>) powder by a biomimetic process. The precipitation was accomplished by immersing TiO<sub>2</sub> powder in simulated body fluid (SBF) for 1, 3, 6, 12 and 24 h. Photocatalytic activity of the apatite-precipitated TiO<sub>2</sub> (HAp-TiO<sub>2</sub>) powders was investigated to assess the decomposition of methylene blue (MB) in aqueous solution and the removal of acetaldehyde gas under UV irradiation. Hydroxyapatite precipitation enhanced the photocatalytic activity of the TiO<sub>2</sub> powder. The time required for the complete degradation of MB decreased from 3.5 to 2 h with the immersion of TiO<sub>2</sub> powders in SBF for 3 h. In terms of acetaldehyde gas decomposition, less than 1 h was sufficient to achieve complete removal for HAp-TiO<sub>2</sub> powder but at least 2 h were required for the bare TiO<sub>2</sub> powder. HAp-TiO<sub>2</sub> powders could therefore be a promising candidate photocatalyst for environmental purification.

**Key words:** TiO<sub>2</sub> powder, Apatite, Simulated Body Fluid, Photocatalyst.

### Introduction

Titanium dioxide (TiO<sub>2</sub>) is of interest for its ability to photodegrade and eliminate many organic and inorganic pollutant chemicals [1–4]. When exposed to ultraviolet (UV) light, the TiO<sub>2</sub> photocatalyst generates an oxidizing effect that eliminates harmful substances by decomposing them into nontoxic materials. Light irradiation of photocatalytic TiO<sub>2</sub> has been already used successfully for the photodegradation of a wide variety of organic compounds [5, 6].

Titanium dioxide is also an attractive material because of its chemical stability, low toxicity, low pollution load, and low cost. However, the utilization of TiO<sub>2</sub> in industrial applications is limited. When blended into organic materials, such as organic paint, textiles, plastics, or paper, TiO<sub>2</sub> tends to decompose these materials photochemically [7, 8]. In addition, due to its lack of ability to attract substances, TiO<sub>2</sub> can only decompose substances that happen to come into contact with it, and its decomposing action fails to work when there is no impinging light [1, 9]. Attempts have been made to improve the photocatalytic activity of TiO<sub>2</sub>. Some experiments have involved reducing the grain size of TiO<sub>2</sub> powder and doping with transition or noble metals [10–12]. Apatite (HAp) coating on the surface of TiO<sub>2</sub> substrates has also been tried using various coating techniques [13, 14]. The HAp has demonstrated efficiency in the absorption of bacteria, viruses, NO<sub>x</sub> and ammonia [15, 16]. Recently, Park [17] produced apatite-precipitated

potassium titanate whiskers and observed that HAp-precipitated whiskers have stronger photocatalytic activity than bare potassium titanate whiskers. However, there is still a need for systematic research into the mechanism of apatite precipitation and its effect on the photocatalytic activity. A better understanding of the photocatalytic activity of HAp-precipitated TiO<sub>2</sub> powders is essential if they are to be technologically useful.

The present study was undertaken to assess the influence of apatite precipitation on the photocatalytic activity of TiO<sub>2</sub> powders. This was evaluated by measuring the decomposition rate of methylene blue (MB) in aqueous solution and the degradation of acetaldehyde gas under UV irradiation. The adsorption-degradation mechanism and kinetics were determined with respect to initial MB and TiO<sub>2</sub> concentrations.

### Experimental Procedure

#### Preparation of HAp-TiO<sub>2</sub> powder

The chemical and physical properties of the commercial photocatalyst TiO<sub>2</sub> (Nano Co., S. Korea, NT-22) are listed in Table 1. Apatite precipitation on the surface of the TiO<sub>2</sub> powder was accomplished by immersing the powders in SBF for 1, 3, and 6 h at 37 °C. The SBF had concentrations of calcium and phosphate ions 10 times greater than those of human blood plasma: hereafter the SBF is termed 10×SBF. The ion concentrations of human blood plasma and the 10×SBF are presented in Table 2. The 10×SBF solution was prepared by dissolving appropriate quantities of analytical-grade chemicals of NaCl, KCl, CaCl<sub>2</sub>·2H<sub>2</sub>O, MgCl<sub>2</sub>·6H<sub>2</sub>O, NaH<sub>2</sub>PO<sub>4</sub> and NaHCO<sub>3</sub> into deionised water,

\*Corresponding author:  
Tel : +82-55-7515325  
Fax: +82-55-7581987  
E-mail: ysheel@yahoo.co.kr

**Table 1.** Chemical and Physical properties of TiO<sub>2</sub> powder used in this study [18]

Component	Value
Crystallinity	Anatase
TiO <sub>2</sub> content (wt%)	> 98.7
Specific Surface Area (m <sup>2</sup> /g)	101.5
1 <sup>st</sup> Particle Size (nm)	20~30
2 <sup>nd</sup> Particle Size (μm)	1~1.5
Appearance Density (g/cc)	0.30~0.35

**Table 2.** Ion concentrations (mM) of blood plasma and 10 × SBF

Media	Na <sup>+</sup>	K <sup>+</sup>	Mg <sup>2+</sup>	Ca <sup>2+</sup>	Cl	HCO <sub>3</sub>	HPO <sub>4</sub> <sup>2-</sup>	SO <sub>4</sub> <sup>2-</sup>
Blood plasma	42.0	5.0	1.5	2.5	103.0	27.0	1.0	0.5
10 × SBF	1010.0	5.0	5.0	25.0	1065.0	10.0	10.0	0

and then buffering at pH 7.4 using tri (hydroxymethyl) aminomethane and 1 M HCl solution. All reagents were analytical grade and used without further purification. After immersion, the powders were removed from the solution, washed with de-ionized water, dried at room temperature, and heat-treated at 200 °C for 0.5 h.

### Characterization

The crystalline phase(s) precipitated on the surface of the TiO<sub>2</sub> powder during immersion in 10×SBF were identified by an X-ray diffractometer, XRD, (Rigaku Geigerflex-DMAX/B). Each sample was scanned from 20 to 50° 2θ at a rate of 2°/minute by 0.02° increments continuously. The crystal morphology of the TiO<sub>2</sub> powders was examined with a scanning electron microscope, SEM (Jeol 6400). Quantitative elemental analyses, specific surface area measurements, and structural analyses of the TiO<sub>2</sub> powders were performed by Energy Dispersive Spectroscopy, EDS, (Noran Instruments), BET surface area analyser (Micromeritics), and Fourier transform infrared spectroscopy, FTIR, (Perkin-Elmer), respectively.

### Photodecomposition of methylene blue (MB)

Photocatalytic activity of the TiO<sub>2</sub> powders immersed in 10×SBF for various durations was determined using an aqueous MB solution. The MB concentration in the aqueous solution was kept constant at 10 mg/l. A 300 ml quantity of the MB solution and 0.3, 0.6, or 1 g of TiO<sub>2</sub> powder was mixed to obtain a suspension. Prior to photo-irradiation, the suspension was magnetically stirred at a constant stirring rate of 500 rpm in the dark for 0.5 h to allow the TiO<sub>2</sub> powders to absorb the MB solution and to establish absorption-desorption equilibrium. Then the suspension was irradiated by a 100 W UV lamp (UVP Co., 360 nm). In order to prevent any light-induced heat, the suspension was cooled with a water-cooling appliance during the entire duration of the test. Every 30 minute analytical samples were taken from the suspension. The UV-vis absorption

rates of the samples were measured at a wavelength of 664 nm, using a UV-vis spectrophotometer (Optima SP-300). The change of absorbance intensity with UV irradiation time was monitored until complete degradation was attained.

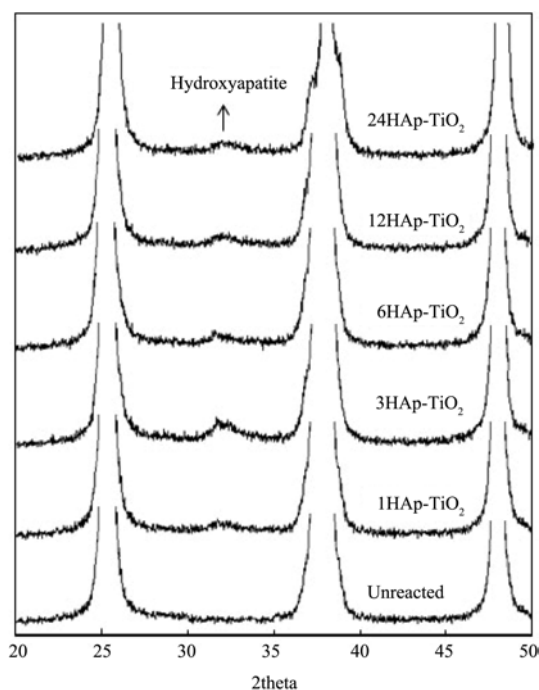
### Gas decomposition test

The decomposition and removal of acetaldehyde gas was measured under UV irradiation to investigate the photocatalytic air purification effects of bare or apatite-precipitated TiO<sub>2</sub> powders. A quantity of 0.5 g of photocatalytic powder was mixed with distilled water and placed on glass Petri-dishes of 100 × 18 mm (diameter × depth) to obtain a flat and homogeneous layer of the photocatalyst. The dishes were placed into a 3 L Tedla bag with an initial concentration of 100 ppm of acetaldehyde gas. Under UV lamp irradiation, the change of acetaldehyde concentration in the Tedla bag was monitored by gas detector tubes (Gastec Co.) every 15 minute for up to 2 h or until complete decomposition was achieved.

## Results and Discussion

### Apatite precipitation on TiO<sub>2</sub> powder

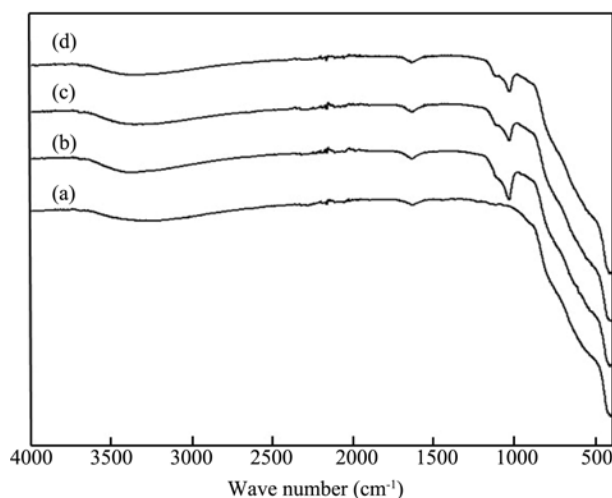
Bare TiO<sub>2</sub> powders and the TiO<sub>2</sub> powders immersed in 10×SBF for 1, 3, 6, 12, and 24 h durations are hereafter referred to as unreacted TiO<sub>2</sub>, 1HAp-TiO<sub>2</sub>, 3HAp-TiO<sub>2</sub>, 6HAp-TiO<sub>2</sub>, 12HAp-TiO<sub>2</sub>, and 24HAp-TiO<sub>2</sub>, respectively, according to their immersion durations in 10×SBF. The XRD patterns of the powders indicate the characteristic (101) diffraction peak of anatase TiO<sub>2</sub> at 2θ~25.3° before and after immersion of the powders in 10×SBF as shown in Fig. 1. A decrease in the intensity of the (101) peak

**Fig. 1.** XRD patterns of TiO<sub>2</sub> powders before and after immersion in 10 × SBF.

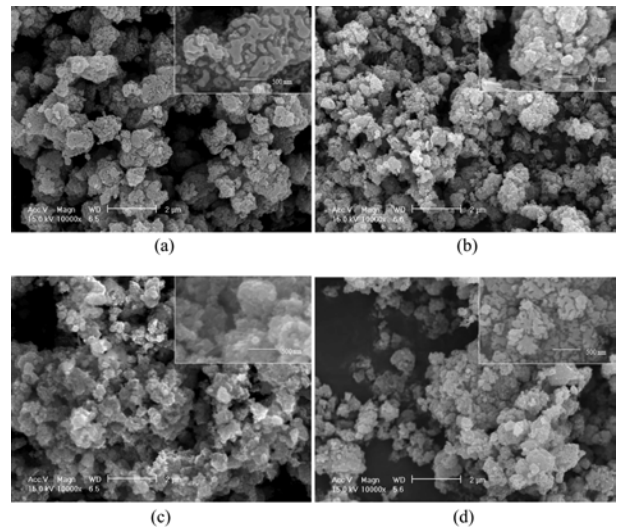
and appearance of new peaks in the diffraction patterns suggest the formation of new phase(s) after immersion. A small but visible diffraction peak at  $2\theta$  of  $\sim 31.6^\circ$  related to the (211) plane of apatite crystals [HAp,  $\text{Ca}_{10}(\text{PO}_4)_6(\text{OH})_2$ ]. The apatite precipitates on the  $\text{TiO}_2$  powders displayed a small crystallite size or a poorly-crystallized structure, judging from the diffraction patterns of the apatite-precipitated  $\text{TiO}_2$  powders. The HAp peak was absent in the XRD pattern of unreacted  $\text{TiO}_2$ . Such results are in good agreement with other researchers [19-21]. The intensity of the HAp peak increased slightly in the  $\text{TiO}_2$  powders immersed in  $10\times\text{SBF}$  up to 3 h, but did not appear to change with further periods of immersion, implying that apatite precipitation on  $\text{TiO}_2$  powders is limited in these immersion conditions and does not increase with increasing immersion durations beyond 3 h. Therefore, the rest of this study was conducted only on unreacted  $\text{TiO}_2$ , 1HAp- $\text{TiO}_2$ , 3HAp- $\text{TiO}_2$ , and 6HAp- $\text{TiO}_2$ .

Fig. 2 shows the FTIR spectra of  $\text{TiO}_2$  powders before and after immersion in  $10\times\text{SBF}$  for various durations. An obvious change in the spectrum was observed after immersion of  $\text{TiO}_2$  powders in  $10\times\text{SBF}$ . The intense and broad bands at  $3370$  and  $1640\text{ cm}^{-1}$  were attributed to the O-H stretching and bending, respectively [19]. Intense bands due to the  $\text{PO}_4^{3-}$  group at  $1000$ - $1100\text{ cm}^{-1}$  were observed in the apatite-precipitated  $\text{TiO}_2$  powders [20]. The narrow bands shown between wavelengths of  $2300$  and  $1800\text{ cm}^{-1}$  correlated to the attenuated total reflectance (ATR) accessory crystal. Absorption peaks at  $1421$  and  $1460\text{ cm}^{-1}$  attributed to carbonate ions [22] were observed in powders immersed in  $10\times\text{SBF}$ . This indicates that the precipitates were composed of HAp only.

Fig. 3 shows the microstructural morphology of  $\text{TiO}_2$  powders. It is evident that apatite precipitates are formed on the surface of  $\text{TiO}_2$  powders on immersion in  $10\times\text{SBF}$ . The surface of unreacted  $\text{TiO}_2$  is clean and smooth as



**Fig. 2.** FTIR spectra of  $\text{TiO}_2$  powders before and after immersion in  $10\times\text{SBF}$ : unreacted  $\text{TiO}_2$ , (b) 1HAp- $\text{TiO}_2$ , (c) 3HAp- $\text{TiO}_2$ , and (d) 6HAp- $\text{TiO}_2$ .



**Fig. 3.** SEM micrographs of (a) the unreacted  $\text{TiO}_2$  powders and the apatite-precipitated  $\text{TiO}_2$  powders after immersion in  $10\times\text{SBF}$  for (b) 1 h, (c) 3 h, and (d) 6 h.

shown in Fig. 3(a), but becomes covered with the apatite precipitates after immersion in  $10\times\text{SBF}$  for 1 and 3 h as best shown in the insets to Figs. 3(b) and (c), respectively. When the immersion duration was increased to 6 h, the surface morphology resembled the morphology of the unreacted  $\text{TiO}_2$  powders as seen in Fig. 3(d). The change in surface morphology with increasing immersion durations could be interpreted as follows: Some amounts of Ca and P ions separated from the  $\text{TiO}_2$  surface, because the change in ion concentrations in the  $10\times\text{SBF}$  induced the Ca and P ions to be re-dissolved. The quantity of apatite precipitates increased to 8.3 weight percentage (wt%) with 3 h of immersion, then decreased to 7.3 wt% with 6 h of immersion. The quantity of apatite precipitates as determined by EDS analysis and the BET specific surface area of the  $\text{TiO}_2$  powders before and after immersion in  $10\times\text{SBF}$  are presented in Table 3. The BET surface area of unreacted  $\text{TiO}_2$  decreased from  $101.5$  to  $78.4\text{ m}^2/\text{g}$  with 3 h of immersion but increased to  $80.2\text{ m}^2/\text{g}$  with 6 h of immersion. We concluded that the ions in the  $10\times\text{SBF}$  solution had filled the fine pores between the  $\text{TiO}_2$  particles, and that nano-sized pores on the  $\text{TiO}_2$  powder's surface were then covered by the apatite precipitates.

EDS analyses of the  $\text{TiO}_2$  powders revealed that Ca and P were present in the apatite-precipitated  $\text{TiO}_2$  powders; Ca/P ratios were 1.39, 1.06, and 1.16 for 1HAp- $\text{TiO}_2$ ,

**Table 3.** Percentage of the apatite precipitates and specific surface area of the  $\text{TiO}_2$  powders

$\text{TiO}_2$ powder	Apatite (wt%)	BET Specific Surface Area ( $\text{m}^2/\text{g}$ )
Unreacted	0	101.5
1HAp- $\text{TiO}_2$	5.9	82.1
3HAp- $\text{TiO}_2$	8.3	78.4
6HAp- $\text{TiO}_2$	7.3	80.2

3HAp-TiO<sub>2</sub> and 6HAp-TiO<sub>2</sub>, respectively. The Ca/P ratios of the apatite precipitates were lower than 1.67- i.e. the ratio in the adult human bone. With longer immersion time, the Ca/P ratio decreased because of the increase of precipitated P ions on the TiO<sub>2</sub> surface. Analysis suggests that the precipitated HAp has calcium-deficient apatite crystal structure.

Consistent with the XRD and FTIR results, SEM and EDS analyses proved that TiO<sub>2</sub> powders could induce the nucleation and growth of apatite and that apatite precipitates could be obtained on TiO<sub>2</sub> powders. When TiO<sub>2</sub> powders are immersed in 10×SBF, apatite nuclei form on them due to the electrostatic interaction between negatively charged TiO<sub>2</sub> surfaces and the ions in the SBF [23]. After nucleation, the apatite formed on the TiO<sub>2</sub> powder becomes the center of nucleation and growth rather than the TiO<sub>2</sub> surface. The calcium ions, phosphate ions and other minor ions (i.e. CO<sub>3</sub><sup>2-</sup> and Mg<sup>2+</sup>) in the SBF solution deposit spontaneously on the TiO<sub>2</sub> surfaces to form apatite precipitates because the SBF solution has been supersaturated with the apatite.

Within the pH range of 7.25-7.40, negatively charged Ti-OH groups are formed on the surface of TiO<sub>2</sub> powders in the SBF solution [19]. Apatite precipitation cannot take place without calcium ions since the Ti-OH groups first combine with a certain number of Ca<sup>2+</sup> ions in the SBF to form a type of calcium titanate. The calcium titanate then combines with the PO<sub>4</sub><sup>3-</sup> ions. Subsequently, large amounts of Ca<sup>2+</sup> and PO<sub>4</sub><sup>3-</sup> ions are adsorbed onto the surface of the TiO<sub>2</sub> powders to form apatite [24]. A schematic illustration of the possible mechanism of apatite precipitation on TiO<sub>2</sub> powder in SBF is shown in Fig. 4.

#### Photocatalytic activity of HAp-TiO<sub>2</sub>

Fig. 5 illustrates the various levels of MB concentration correlated with duration of UV irradiation for the unreacted and apatite-precipitated TiO<sub>2</sub> powders. It is apparent that all powders are active in the photocatalytic decomposition of MB. When the samples were kept in the dark for 0.5 h, the amount of MB removed by the apatite-precipitated TiO<sub>2</sub> powders was greater than for the unreacted TiO<sub>2</sub> powder which absorbed only 11.7% of MB. The amount

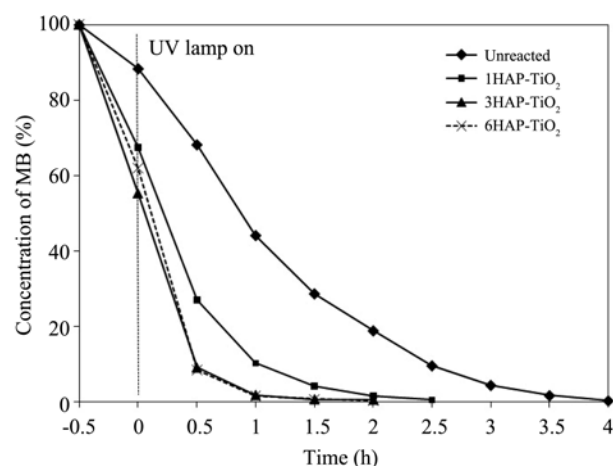


Fig. 5. Photocatalytic degradation of the unreacted and apatite-precipitated TiO<sub>2</sub> powders.

of MB absorbed in the dark by 1HAp-TiO<sub>2</sub>, 3HAp-TiO<sub>2</sub> and 6HAp-TiO<sub>2</sub> was 32.6%, 44% and 38%, respectively. The absorbability of TiO<sub>2</sub> powders increased with increasing additions of apatite precipitates. The complete decomposition of MB was achieved after 4 h exposure to UV illumination for unreacted TiO<sub>2</sub> but this time decreased to 2.5 h for 1HAp-TiO<sub>2</sub>, and to 2 h for 3HAp-TiO<sub>2</sub>. The complete decomposition of MB for 6HAp-TiO<sub>2</sub> was achieved in a time very similar to that of 3HAp-TiO<sub>2</sub>. The photocatalytic performance of HAp-TiO<sub>2</sub> was much better than that of the unreacted TiO<sub>2</sub>, despite deficiency in BET surface area. Similar results have been obtained by Anmin *et al.* [25] who explained that the strong adsorption of the intermediates on HAp and their subsequent transfer to TiO<sub>2</sub> may induce a photocatalytic synergy. Yun *et al.* [26] observed beneficial photocatalytic side-effects in carbon-coated TiO<sub>2</sub> and explained that the adsorption of the pollutants on activated carbon and the mass transfer to photocatalytic TiO<sub>2</sub> induced effective degradation because of a common interface between the carbon and TiO<sub>2</sub>.

The photocatalytic degradation of MB in the presence of HAp-TiO<sub>2</sub> could be described in terms of a first-order kinetic Langmuir-Hinshelwood mechanism [27-29].

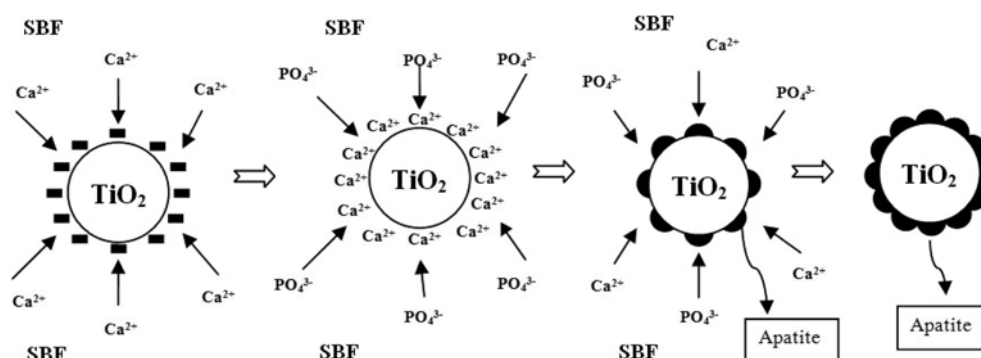


Fig. 4. Schematic diagram showing the possible mechanism of apatite formation on TiO<sub>2</sub> powder in 10 × SBF.

$$\ln\left(\frac{MB_0}{MB_t}\right) = k_{ap}t \quad (1)$$

where  $k_{ap}$  is the apparent reaction rate constant, and  $MB_0$  and  $MB_t$  are, respectively, the concentrations of MB at time 0 and at time  $t$ . The  $k_{ap}$  is calculated from the slope of the  $\ln([MB]_0/[MB])$  versus UV irradiation time curve as shown in Fig. 6. The values of  $k_{ap}$  for the TiO<sub>2</sub> powders are listed in Table 4. The  $k_{ap}$  value of HAp-TiO<sub>2</sub> is higher than that of unreacted TiO<sub>2</sub> and the highest  $k_{ap}$  value is obtained for 3HAp-TiO<sub>2</sub>. The apatite precipitates on the surface of TiO<sub>2</sub> increases the kinetic activity of MB decomposition since the apatite precipitation attracts the pollutants. As seen in Table 4, the correlation coefficients ( $R^2$ ) have high values, implying that the decomposition of MB in this study was obeying the first-order kinetic Langmuir-Hinshelwood mechanism model.

### Photocatalyst effects

Photocatalytic effects were investigated by varying the amount of 3HAp-TiO<sub>2</sub> in the MB solution between 0.3, 0.6, and 1.0 g/l. The variations in MB concentration versus UV irradiation-times are illustrated in Fig. 7. The amount of MB adsorbed in the dark was 44% for 0.3 g/l of 3HAp-TiO<sub>2</sub>, but rose to 51% and 59% for 0.6 and 1.0 g/l of 3HAp-TiO<sub>2</sub>, respectively. The results reveal that photocatalytic activity increases with the amount of photocatalyst in the MB solution. The complete decomposition of MB was achieved after 2 h of UV illumination with 0.3 g/l of 3HAp-TiO<sub>2</sub>, but this time decreased to

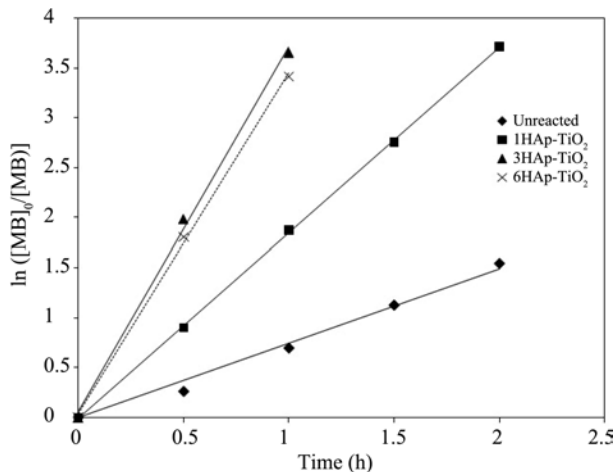


Fig. 6. The variation of  $\ln([MB]_0/[MB])$  versus UV irradiation time.

Table 4. The reaction rate constants and correlation coefficients for the photocatalytic decomposition of MB.

TiO <sub>2</sub> Powder	$k_{ap}$ (h <sup>-1</sup> )	$R^2$
Unreacted	0.7454	0.9885
1HAp-TiO <sub>2</sub>	1.8595	0.9995
3HAp-TiO <sub>2</sub>	3.6549	0.9989
6HAp-TiO <sub>2</sub>	3.4128	0.9975

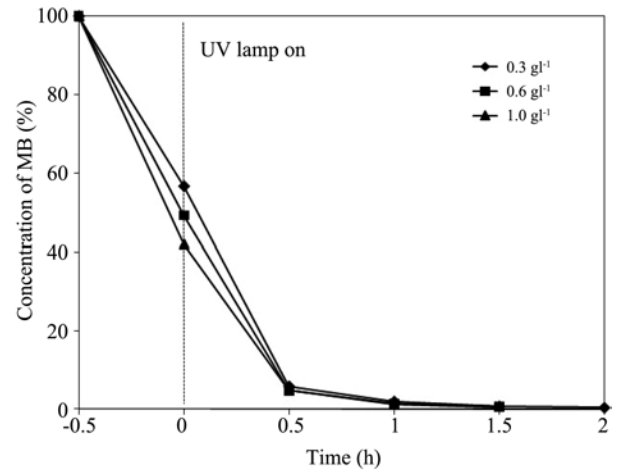


Fig. 7. Photocatalytic degradation of 3HAp-TiO<sub>2</sub> versus UV irradiation time.

1.5 h when 0.6 or 1.0 g/l of 3HAp-TiO<sub>2</sub> was used. Degradation efficiency improved with increasing apatite-precipitated TiO<sub>2</sub> powder concentration, a result attributable to the increase in total surface area available for contaminant adsorption. Results indicate that the apatite precipitates attract foreign substances and this enhances photocatalytic activity.

### Absorption isotherms

It has been observed that apatite precipitates absorb MB even in the dark. Adsorption of pollutants is an important parameter in determining the photocatalytic degradation rate. Adsorption data obtained in the dark were assessed to find the equilibrium constants of the adsorption of the dye on the surface of the 3HAp-TiO<sub>2</sub> photocatalyst. According to Langmuir isotherms, the rate of adsorption will increase with increasing concentrations of an adsorbate. However, once sites are occupied, a further increase in adsorbate concentration will not increase the adsorbed amount; that is, the saturation point is reached.

The experimental data was fitted to the Langmuir equation (equation (2)) to describe the adsorption of MB on the surface of the 3HAp-TiO<sub>2</sub> photocatalyst:

$$Y = \frac{KC_e}{1 + KC_e} \quad (2)$$

where  $Y$  is the fraction of the photocatalyst surface covered by adsorbed MB molecules;  $K$  is the Langmuir equilibrium constant;  $C_e$  is the MB equilibrium concentration. Alternatively,

$$Y = \frac{X_e}{X_m} \quad (3)$$

where  $X_e$  represents the mg of MB adsorbed per gram of 3HAp-TiO<sub>2</sub> at equilibrium concentration,  $C_e$ .  $X_m$  is the mass of MB (mg) per gram of 3HAp-TiO<sub>2</sub> needed to form a monolayer. The linear transformation of equation (2) can be expressed by the following equation:

$$\frac{C_e}{X_e} = \frac{C_e}{X_m} + \frac{1}{KX_m} \quad (4)$$

From the MB adsorption isotherm, the plot  $C_e/X_e$  versus  $C_e$  gives a straight line ( $R^2 = 0.9995$ ) with a slope of  $1/X_m$  (0.0121) and the interception with the x-axis of  $1/KX_m$  (0.0759) as shown in Fig. 8. The results confirm that the Langmuir isotherm is appropriate to describe the adsorption of MB onto the surface of 3HAp-TiO<sub>2</sub>. The required amount of MB (mg per gram of 3HAp-TiO<sub>2</sub>) to form a monolayer ( $X_m$ ) is 82.64. The Langmuir adsorption constant ( $K$ ) is 0.1613. The specific surface area can be estimated by the following equation:

$$S_{MB} = \frac{X_M \times a_{MB} \times N}{M} \quad (5)$$

where  $S_{MB}$  is the specific surface area in m<sup>2</sup>/g;  $X_m$  is the quantity of MB molecules adsorbed at the monolayer;  $a_{MB}$  is the occupied surface area of one molecule of MB ( $0.55 \times 10^{-18}$  m<sup>2</sup>); [29, 30]  $N$  is the Avogadro constant ( $6.02 \times 10^{23}$  /mol);  $M$  is the molecular weight of MB (g mol<sup>-1</sup>). The value calculated for the specific surface area is 73.2 m<sup>2</sup>/g, which agrees with the value determined by the BET method (78.4 m<sup>2</sup>/g), as presented in Table 3.

### Photocatalytic removal of acetaldehyde gas

The decomposition rates of acetaldehyde gas with different UV irradiation times and for a variety of photocatalysts are illustrated in Fig. 9. All photocatalysts were active in the photocatalytic decomposition of acetaldehyde. The complete removal and degradation of acetaldehyde was attained after 2 h of UV irradiation for unreacted TiO<sub>2</sub>. The time for the complete removal and degradation of acetaldehyde decreased to less than 1 h when 3HAp-TiO<sub>2</sub> and 6HAp-TiO<sub>2</sub> powders were used. These results reveal that the apatite precipitates enhances the photocatalytic activity of TiO<sub>2</sub> powders through the ability of the precipi-

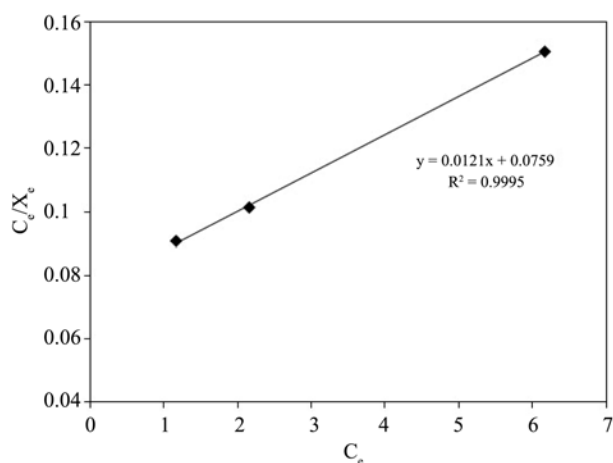


Fig. 8. The plot  $C_e/X_e$  versus  $C_e$  for 3HAp-TiO<sub>2</sub>.

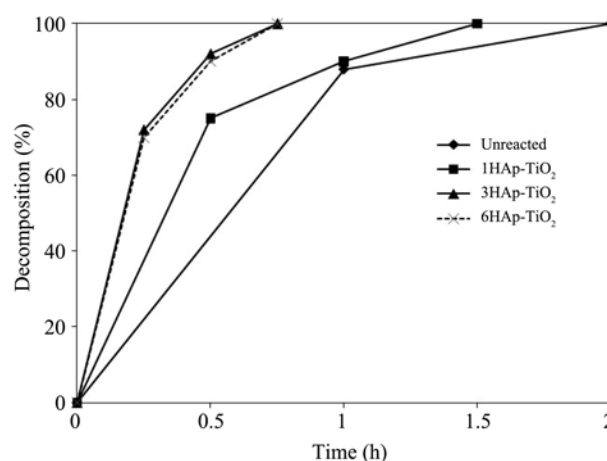


Fig. 9. Variation in decomposition rate of acetaldehyde with UV irradiation time for the unreacted and apatite-precipitated TiO<sub>2</sub> powders.

itated apatite phase to absorb air pollutants [9, 27]. The synergistic effect of the HAp-TiO<sub>2</sub> photocatalyst may be due to the strong absorption of the intermediates on HAp and to their subsequent transfer to TiO<sub>2</sub>.

### Conclusions

Apatite-precipitated TiO<sub>2</sub> could be successfully synthesized by using a simple and low cost biomimetic process. Apatite precipitation enhanced the adsorbability of TiO<sub>2</sub> powders in the dark; it also influenced photocatalytic activity in methylene blue (MB) solution and the removal of acetaldehyde gas under UV irradiation. We found a correlation between the absorption of MB onto apatite-precipitated TiO<sub>2</sub> and the rate of degradation of MB. The photocatalytic degradation was evidently affected by the initial concentration of the photocatalyst in accordance with the Langmuir-Hinshelwood kinetic model. Apatite-precipitated TiO<sub>2</sub> powders could therefore be a promising candidate photocatalyst for environmental purification.

### Acknowledgements

This work was jointly supported by the Scientific and Technical Research Council of Turkey, TUBITAK, project number : 106M531 and by the Korea Research Foundation, KRF, project number : KRF-2006-033-D00010. The authors are grateful to TUBITAK and KRF.

### References

1. A. Fujishima, T.N. Rao and D.A. Tryk, J. Photochem. Photobiol. C: Photochem. Rev. 1 (2000) 1-21.
2. O. Legrini, E. Oliveros and A. Braun, Chem. Rev. 93 (1993) 671-698.
3. F. Kskadar, A.B.D. Nandiyanto, K.M. Yun, C.J. Hogan, K. Okuyama and P. Biswas, Adv. Mater. 19 (2007) 1408-1412.
4. M. Kang, Y.R. Ko, M.K. Jeon, S.C. Lee, S.J. Choung, J.Y. Park, S. Kim and S.H. Choi, J. Photochem. Photobiol. A:

- Chem. 173 (2005) 128-136.
5. G. Chen, G. Luo, X. Yang, Y. Sun and J. Wang, *Mater. Sci. Eng. A* 380 (2004) 320-325.
  6. I.K. Konstantinou and T.A. Albanis, *Appl. Catal. B: Environ.* 49 (2004) 1-14.
  7. W.A. Daoud, J.H. Xin and Y.H. Zhang, *Surf. Sci.* 599 (2005) 69-75.
  8. X.Z. Li, F.B. Li, C.L. Yang and W.K. Ge, *J. Photochem. Photobiol. A. Chem.* 141 (2001) 209-217.
  9. T. Nonami, H. Hase and K. Funakoshi, *Catal. Today* 96 (2004) 113-118.
  10. S.H. Woo, W.W. Kim, S.J. Kim and C.K. Rhee, *Mater. Sci. Eng. A* 449-451 (2007) 1151-1154.
  11. Y. Su, Y. Xiao, X. Fu, Y. Deng and F. Zhang, *Mater. Res. Bull.* 44 (2009) 2169-2173.
  12. H. Tian, J. Ma, K. Li and J. Li, *Mater. Chem. Phys.* 112 (2008) 47-51.
  13. M. Iwasaki, Y. Miyamoto, S. Ito, T. Furuzono and W.-K. Park, *J. Colloid Interface Sci.* 326 (2008) 537-540.
  14. S. Aryal, S.R. Bhattarai, R. Bahadur K.C., M.S. Khil, D.R. Lee and H.Y. Kim, *Mater. Sci. Eng. A* 426 (2006) 202-207.
  15. K. Elkabouss, M. Kacimi, M. Ziyad, S. Ammar and F. Bozon-Verduraz, *J. Catal.* 226 (2004) 16-24.
  16. Y. Watanabe, Y. Moriyoshi, Y. Suetsugu, T. Ikoma, T. Kasama, T. Hashimoto, H. Yamada and J. Tanaka, *J. Am. Ceram. Soc.* 87 (2004) 1395-1397.
  17. J. Park, *J. Alloys Compd.* 492 (2010) L57-L60.
  18. NANO Co. brochure, Jinju, Korea
  19. Z. Yang, S. Si, X. Zeng, C. Zhang and H. Dai, *Acta Biomater.* 4 (2008) 560-568.
  20. T. Kasuga, H. Kondo and M. Nogami, *J. Crystal Growth* 235 (2002) 235-240.
  21. M. Keshmiri, T. Troczynski and J. Non-Crystalline Solids 324 (2003) 289-294.
  22. S. Masmoudi, A. Larbot, H. El Feki and R. Ben Amar, *Desalination* 190 (2006) 89-103.
  23. Y.W. Gu, B.Y. Tay, C.S. Lim and M.S. Yong, *Biomaterials* 26 (2005) 6916-6923.
  24. T. Miyazaki, H.-M. Kim, T. Kokubo, C. Ohtsuki, H. Kato and T. Nakamura, *Biomaterials* 23 (2002) 827-832.
  25. H. Anmin, L. Tong, C. Chengkang, L. Huiqin and M. Dali, *Appl. Catal. B: Environ.* 63 (2006) 41-44.
  26. S.M. Yun, K. Palanivelu, Y.H. Kim, P.H. Kang and Y.S. Lee, *J. Indust. Eng. Chem.* 14 (2008) 667-671.
  27. R. Khan, S.W. Kim, T.J. Kim and C.M. Nam, *Mater. Chem. Phys.* 112 (2008) 167-172.
  28. G. Zhang, X. Zou, J. Gong, F. He, H. Zhang, Q. Zhang, Y. Liu, X. Yang and B. Hu, *J. Alloys Compd.* 425 (2006) 76-80.
  29. N. Barka, A. Assabbane, A. Nounah and Y.A. Ichou, *J. Hazard. Mater.* 152 (2008) 1054-1059.
  30. L.M. He and B.M. Tebo, *Appl. Environ. Microbiol.* 64 (1998) 1123-1129.